Science
AAAS

# Video-Rate Far-Field Optical Nanoscopy Dissects Synaptic Vesicle Movement

Volker Westphal, *et al.*

*Science* **320**, 246 (2008);
DOI: 10.1126/science.1154228

doubly dehydrated (**6**) while still tethered to the protein. The complex intermediates were confirmed by the observation of each specific phosphopantetheinyl ejection ion within 1.5 ppm (*14*). These phosphopantetheinyl ejection ions were further subjected to ion trap fragmentation to provide data corroborating their proposed structures (figs. S5 to S9).

Apart from the relative populations of the fully extended polyketide intermediates, both two-part combination reactions gave remarkably similar outcomes (Fig. 4). Elaboration of only the hexanoyl-primed ACP, and not the acetyl-primed (from KS-mediated loss of $CO_2$ from malonyl) or malonyl-primed ACP, supports the notion that the KS domain exerts control over the selection and extension of only specific starter units tethered to the ACP domain (in this case hexanoyl-*S*-ACP). These data support the assertion that the PT domain maintains the correct intramolecular aldol addition intermediate and promotes its dehydration, facilitating nonenzymatic release of either the naphthopyrone **5** or the anthrone **2**. Note that the ACP active-site tryptic peptide with the doubly dehydrated hexanoate + 7 acetate species (**6**, PT product) showed an absorbance under single-wavelength analysis (310 nm), in further support that this species is indeed the TE/CLC substrate. Combined with the drastic reduction in the flux to product(s) in the absence of the tailoring domains (Fig. 2), the mass spectrometric data support assignment of the PT domain as an aromatase/cyclase domain.

The deconstruction approach taken here has demonstrated the synthetic roles of all recognized domains in an IPKS catalytic cycle, notably the product template (PT) domain, which should prove to be general for the broad class of multidomain IPKSs. The insights afforded by the catalytic autonomy of these dissected, free-standing domains enable a rational strategy for engineering these enzymes to synthesize alternative products.


**References and Notes**

1. J. Staunton, K. J. Weissman, *Nat. Prod. Rep.* **18**, 380 (2001).
2. M. A. Fischbach, C. T. Walsh, *Chem. Rev.* **106**, 3468 (2006).
3. J. M. Crawford, A. L. Vagstad, K. C. Ehrlich, C. A. Townsend, *Bioorg. Chem.* **36**, 16 (2008).
4. D. Udwary, M. Merski, C. A. Townsend, *J. Mol. Biol.* **323**, 585 (2002).
5. J. M. Crawford, B. C. R. Dancy, E. A. Hill, D. W. Udwary, C. A. Townsend, *Proc. Natl. Acad. Sci. U.S.A.* **103**, 16728 (2006).
6. C. Sanchez, L. Du, D. J. Edwards, M. D. Toney, B. Shen, *Chem. Biol.* **8**, 725 (2001).
7. I. Fujii, A. Watanabe, U. Sankawa, Y. Ebizuka, *Chem. Biol.* **8**, 189 (2001).
8. Z.-G. Chen, I. Fujii, Y. Ebizuka, U. Sankawa, *Phytochem* **38**, 299 (1995).
9. R. McDaniel, S. Ebert-Khosla, D. A. Hopwood, C. Khosla, *Science* **262**, 1546 (1993).
10. Y. Tang, S. C. Tsai, C. Khosla, *J. Am. Chem. Soc.* **125**, 12708 (2003).
11. A. T. Keatinge-Clay, D. A. Maltby, K. F. Medzihradszky, C. Khosla, R. M. Stroud, *Nat. Struct. Mol. Biol.* **11**, 888 (2004).
12. Y. Ma *et al.*, *ChemBioChem* **7**, 1951 (2006).
13. S. M. Ma *et al.*, *J. Am. Chem. Soc.* **130**, 38 (2008).
14. P. C. Dorrestein *et al.*, *Biochemistry* **45**, 12756 (2006).


15. Supported by NIH research grants ES001670 (C.A.T.) and GM067725 (N.L.K.), NIH Chemical Biology Interface training grant GM070421 (P.M.T.), and NIH postdoctoral fellowship GM079408 (J.R.S.).


**Supporting Online Material**

www.sciencemag.org/cgi/content/full/320/5873/243/DC1
Materials and Methods
Figs. S1 to S9
Tables S1 and S2
References


31 December 2007; accepted 29 February 2008
10.1126/science.1154711


# Video-Rate Far-Field Optical Nanoscopy Dissects Synaptic Vesicle Movement


**Volker Westphal,[1]* Silvio O. Rizzoli,[2,3]* Marcel A. Lauterbach,[1] Dirk Kamin,[3] Reinhard Jahn,[2] Stefan W. Hell[1]†**



We present video-rate (28 frames per second) far-field optical imaging with a focal spot size of 62 nanometers in living cells. Fluorescently labeled synaptic vesicles inside the axons of cultured neurons were recorded with stimulated emission depletion (STED) microscopy in a 2.5-micrometer by 1.8-micrometer field of view. By reducing the cross-sectional area of the focal spot by about a factor of 18 below the diffraction limit (260 nanometers), STED allowed us to map and describe the vesicle mobility within the highly confined space of synaptic boutons. Although restricted within boutons, the vesicle movement was substantially faster in nonbouton areas, consistent with the observation that a sizable vesicle pool continuously transits through the axons. Our study demonstrates the emerging ability of optical microscopy to investigate intracellular physiological processes on the nanoscale in real time.


Many questions in the life sciences could be answered if lens-based optical microscopy featured the resolution of electron microscopy, or if the electron microscope operated under physiological conditions. However, for reasons deeply rooted in the working principles of these systems, nanoscale resolution and noninvasive cellular imaging seemed mutually incompatible. Although widely accepted for decades, this notion is rapidly changing. Particularly in fluorescence imaging, far-field optical concepts have emerged that are no longer limited by diffraction (*1*–*9*). For example, stimulated emission depletion (STED) microscopy (*1*, *2*) overcomes the diffraction barrier by producing fluorescent focal spots smaller than $D \approx 200$ to 300 nm in diameter. In a typical STED microscope, the focal spot of excitation light is overlapped with a doughnut-shaped spot of light of lower photon energy, quenching excited molecules in the excitation spot periphery by stimulated emission. The net result is a subdiffraction-sized fluorescent spot of diameter $d \approx D/\sqrt{1 + I/I_s} < D$, which, if scanned through the specimen, renders images of subdiffraction resolution $d$. $I$ and $I_s$ denote the intensity of the STED beam and the characteristic intensity for the quenching of the fluorescent dye used, respectively. Adjusting $I >> I_s$ allows one to tune the resolution $d$, in principle to the molecular scale.

Until now, the 20- to 70-nm resolution realized with STED has been used to map the nanoscale distribution of proteins inside cells (*3*) and on the plasma membrane (*2*). However, in all of these applications, the cells were fixed or basically static, leaving open the question of whether nanoscale imaging of fast physiological phenomena would be possible. Besides, the fast recording of high-resolution image frames is questionable given the limited number of photons emitted during the frame time. To meet these challenges, we balanced the resolution $d$, tuning the spot down to a size at which we were able to collect just enough photons from the features of interest to safely discern them from background. This strategy, a special feature of STED microscopy and related techniques (*7*), allowed reliable repeated imaging of rapidly moving small organelles inside living cells with nanoscale resolution. Specifically, we investigated the movement of synaptic vesicles in cultured neurons.

Although several steps in synaptic vesicle recycling are well understood (*10*), vesicle movement has been difficult to study, because the ~40-nm-diameter vesicles are housed in presynaptic nerve terminals of ~1 μm in diameter, referred to as synaptic boutons. Most current insights have therefore been gained by sparse vesicle labeling (*11*–*13*), or by indirect methods, such as fluorescence recovery after photobleaching (*14*–*16*) and correlation spectroscopy (*17*–*19*).


[1]Department of NanoBiophotonics, Max-Planck-Institute for Biophysical Chemistry, Göttingen 37077, Germany. [2]Department of Neurobiology, Max-Planck-Institute for Biophysical Chemistry, Göttingen 37077, Germany. [3]STED Microscopy of Synaptic Function, European Neuroscience Institute, Göttingen 37077, Germany.

*These authors contributed equally to this work.
†To whom correspondence should be addressed. E-mail: shell@gwdg.de

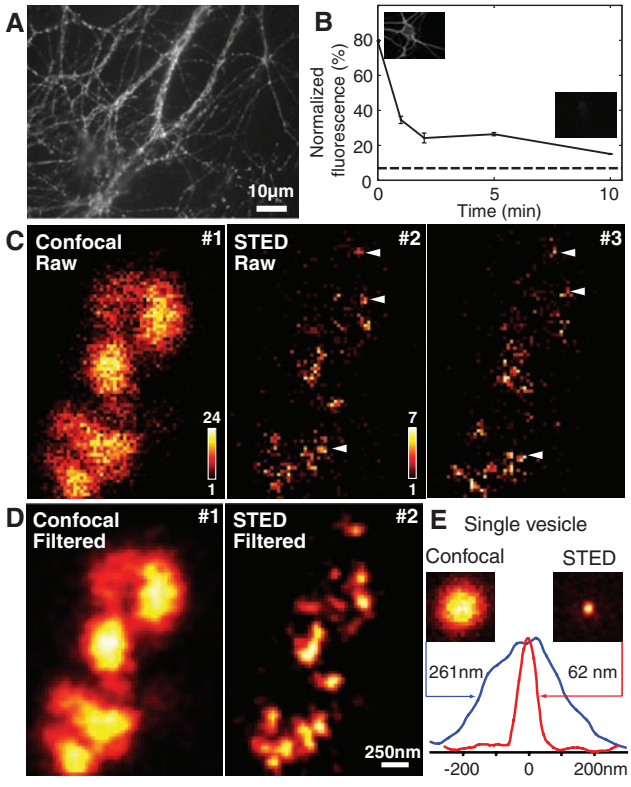


**Fig. 1.** Real-time STED microscopy resolves single synaptic vesicles in living neurons. (**A**) Typical wide-field overview of cultured hippocampal neurons whose surface vesicle pool was labeled with mouse anti-synaptotagmin and Atto647N-labeled anti-mouse Fab fragments. (**B**) The labeled pool of vesicles is rapidly endocytosed, as observed by the reduced number of surface-exposed synaptotagmin molecules with increasing time between primary and secondary antibody labeling (*20*). Data are shown as the mean ± SEM, with each data point representing three to seven independent neuronal cultures. The dashed line indicates the background fluorescence determined from unstained preparations. (**C**) Images of a short fragment of a stained axon, in confocal mode (frame #1) and in STED mode (frames #2 and #3). The increased resolution in the STED image and the reappearance of vesicles in subsequent frames can be seen (three arrowheads indicate relatively stable vesicles; also, many other spots can be recognized in both frames). The insers in #1 and #2 indicate the color maps used. (**D**) Smoothing in confocal mode does not improve the differentiation of single objects, although this filtering method helps to identify superresolved vesicles in the STED images. (**E**) Images of a single stationary vesicle in confocal and STED mode (summed over 10 and 50 frames, respectively) reveal the cross-section of the focal spot in each mode. The line profiles through their center demonstrate the reduction in focal spot area by a factor of 18.

Higher spatial resolution enables the imaging of a sizable fraction of the vesicles simultaneously. We labeled cultured hippocampal neurons with monoclonal mouse antibodies directed against the intravesicular (lumenal) domain of the synaptic vesicle protein synaptotagmin (*2*). The antibodies were briefly applied to the neurons (on ice), followed by an exposure to Fab fragments from antibodies to mouse (anti-mouse) labeled with the organic fluorophore Atto 647N featuring $I_s \approx 10$ to 20 MW/cm$^2$ at a de-excitation wavelength of 750 nm. This procedure ensured that only vesicles fused to the plasma membrane were labeled (*2*), because only these vesicles were exposed to the outside space [Fig. 1A and (*20*)]. The labeled vesicle pool encompassed as much as 10 to 20% of all vesicles (*21*); moreover, this pool fully participated in active vesicle recycling, as confirmed by the rapid endocytosis of the label (Fig. 1B). Two minutes after labeling, only ~18% of the label still resided on the surface; after 10 min, the value had dropped to ~8%.

Figure 1C shows that, unlike standard confocal imaging, STED microscopy enables the detection of single synaptic vesicles. Video-rate imaging was accomplished by scanning the excitation and depletion beam pair in the focal plane by means of a 16-kHz resonant mirror in one direction; the perpendicular axis was scanned by moving the sample with a piezo actuator (*22*). This configuration allowed us to image an 1.8 μm by 2.5 μm area within 35 ms, i.e., at 28 frames per second [movie S1 and (*20*)]. By imaging the fluorescence onto a pinhole and acquiring images rapidly, noise levels were only ~0.1 and 0.02 counts per pixel inside and outside the axons, respectively (Fig. 1C). Although a single detected pho-

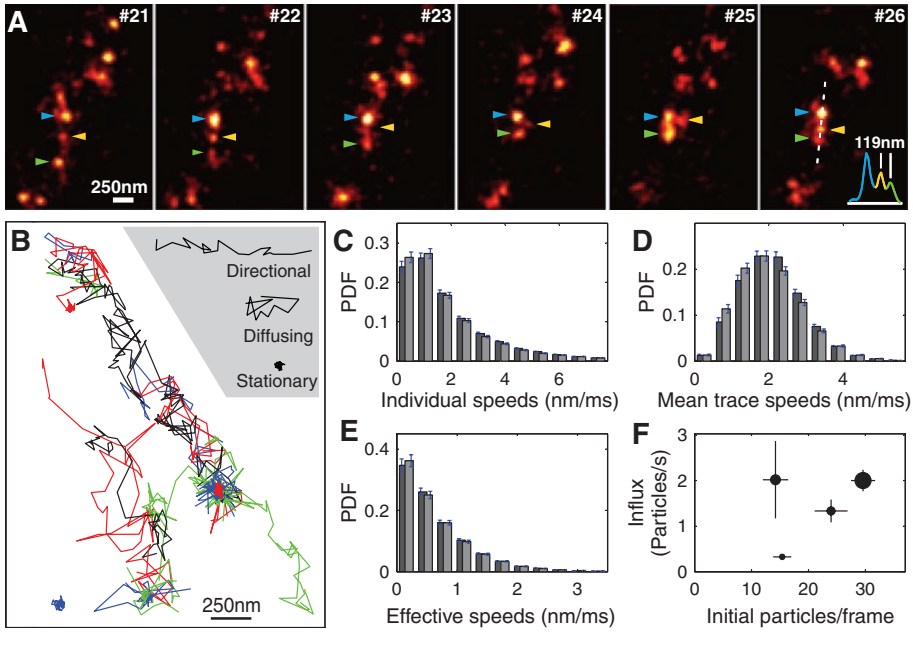


**Fig. 2.** Characteristics of synaptic vesicle movement. (**A**) Successive STED frames, filtered (movie S1). The arrowheads indicate three vesicles, which were tracked in all frames, localized in a subdiffraction space. The inset in frame #26 shows an intensity profile along the dotted white line. (**B**) Example vesicle traces in one movie. Occasionally, vesicles may seem trapped in a small area, whereas other traces are reminiscent of active transport (examples in inset). (**C** to **E**) Histograms of vesicle speeds: (C) based on displacement between two consecutive frames, (D) mean speed per trace, and (E) effective speed determined by dividing the distance between the end and the origin of the trace by the trace duration. See (*20*) for details of the analysis. The results are shown as the mean ± SEM, with movies analyzed from four independent experiments. Black bars show results with normal buffer (53 movies); depolarized preparations (Tyrode solution containing 70 mM KCl) are shown in gray (75 movies). (**F**) Number of vesicles (traces) entering the imaged area per second, as a function of the number of vesicles detected in the first frames of the movie. Results from four independent experiments, each consisting of a number of movies, are shown. The circle area is proportional to the number of movies analyzed. PDF: probability density function (probability normalized to unity).

ton in a pixel could still be due to noise, the probability of simultaneously detecting three or more photons is several standard deviations above the noise level, allowing us to conclude that the detected signal originates from labeled features. This reasoning was confirmed by comparing consecutive frames, where the labeled objects moved only slightly (Fig. 1C, middle and right panels); random noise, by contrast, would manifest itself as flickering. We also measured the frequency of false-positive identifications in preparations where no specific signal was expected (*20*); we found it to be on average around 0.1 events per frame. Applying $I = 400$ MW/cm$^2$ renders a full width at half maximum (FWHM) of our vesicle images of 62 nm (Fig. 1E), which means that the effective focal detection area is reduced by a factor of 18 compared to confocal imaging.

To further improve the confidence of vesicle recognition in our data, we applied a mathematical filter (Fig. 1D), which was essentially a smoothing algorithm. The resolution enhancement, coupled with the filter, allowed us both to observe individual vesicle movements (Fig. 2A) and to track individual vesicles automatically [Fig. 2B and (*20*)]. Although bleaching did occur during data acquisition (fig. S1), we were able to trace large numbers of vesicles, in ~130 movies of 1000 frames each, from four independent experiments. Although the vesicles resided mainly in a low-mobility state (Fig. 2C) (*14*, *15*), most traces also included rapid movements, with the average speed for each individual vesicle peaking around ~2 nm/ms (Fig. 2D).

Because the movement was largely nondirectional, overall vesicle displacement appeared to be restricted (Fig. 2E). In agreement with previous observations, in which mobility was low also during synaptic activity (*13*), none of the mobility parameters increased substantially during stimulation with increased concentrations of KCl. To determine whether vesicle movement was diffusive or motor-driven, we perturbed cytoskeletal elements by using the actin-disrupting agent latrunculin A, or via the microtubule-disrupting nocodazole. The results (fig. S2) show that both drugs reduce vesicle mobility, indicating that active transport plays a role in vesicle traffic in axons. Nevertheless, vesicle motion persisted, suggesting that a substantial fraction of the vesicle movement is diffusive.

Even after bleaching the vesicles that were initially present (fig. S1), fluorescence persisted as new vesicles continuously entered the imaged area, at a rate of 0.5 to 3 vesicles per second in different experiments (Fig. 2F). This result, even taken at its lowest value, indicates that a fairly large number of vesicles passes constantly through the boutons [see also (*23*)].

As a control, we also imaged and analyzed the vesicles in chemically fixed neurons, in which case the vesicle movement was substantially reduced (fig. S3). We occasionally observed vesi-

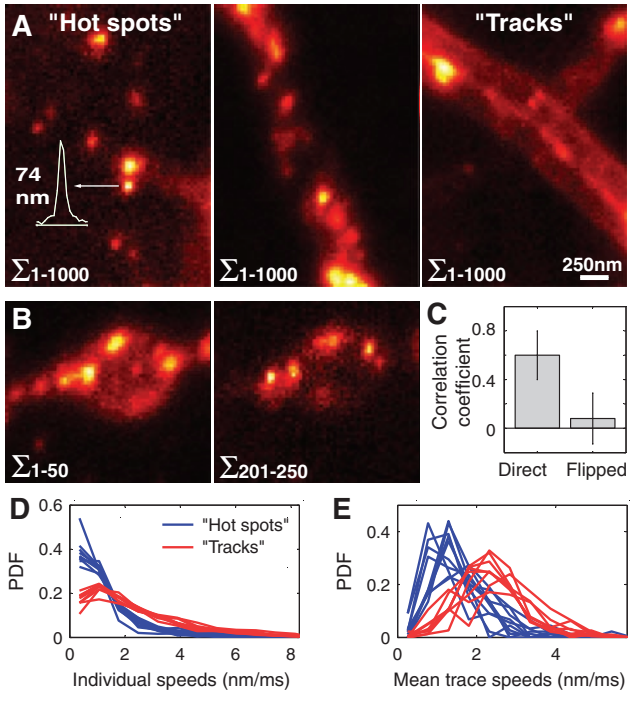


**Fig. 3.** Synaptic vesicle movement in different axonal areas. (**A**) Summing all frames of the individual movies indicates vesicle traces. In many movies, the vesicles seemed to concentrate in "hot spots" (left), which typically assemble in what resembles confocal images of presynaptic boutons. However, other movies showed few spots and were instead dominated by the presence of linear "tracks" of vesicle movement (right). The center panel shows an example of intermediate behavior. The inserted graph displays the intensity profile (with its FWHM) through the hot spot indicated by the thin white arrow. (**B**) The areas preferred by the vesicles are relatively constant. The sums of the first 50 frames (left), and of the frames 201 to 250 (right), are surprisingly similar for the same movie. (**C**) A correlation coefficient analysis between these images performed for all of our movies shows that the areas of vesicle movement tend to correlate (bars show mean ± SD, $n > 100$ images, from four independent experiments). Controls with horizontally flipped images exhibited a substantially reduced correlation. (**D** and **E**) Histograms of individual speeds (D) and mean trace speeds (E) for 8 to 10 different movies dominated by hot spots or tracks.

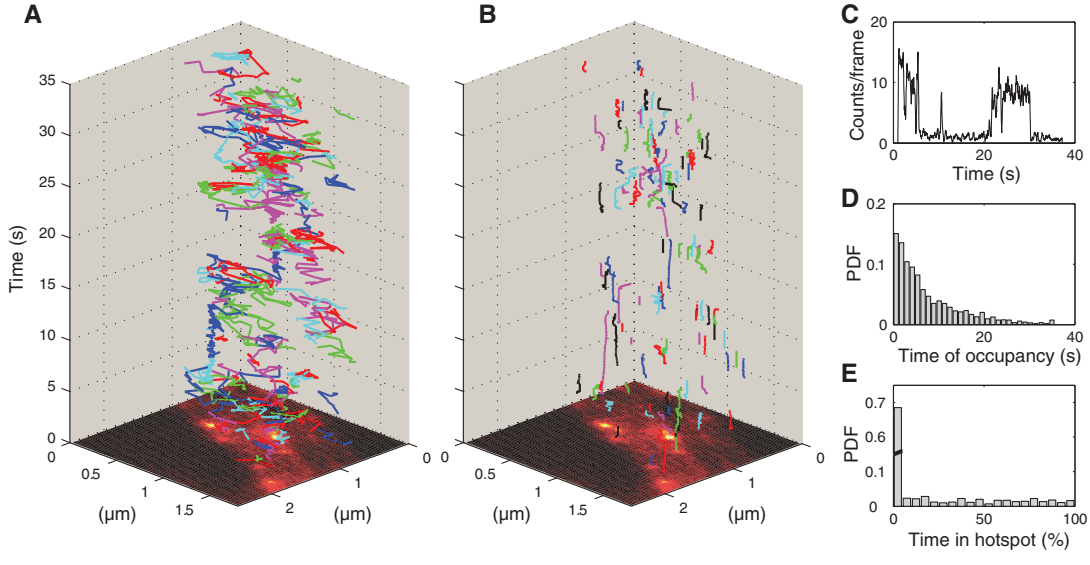


**Fig. 4.** Hot spots of vesicle localization. Comparison between synaptic vesicle traces (**A**) and hot spot traces (**B**). Hot spots were defined as pointlike objects appearing in a 50-frame moving average; they indicate small areas where fluorescence occurs over longer times (*20*). The average image of the complete movie is placed at the bottom. (**C**) Vesicles can move in and remain trapped in hot spots, as shown here by the strong signal fluctuation in a single hot spot. (**D**) Probability histogram of the occupancy time of the hot spots (the fraction of time they were filled by vesicles). (**E**) Histogram of the percentage of time each vesicle spent in a hot spot.

cles instantly losing their fluorescence and then reappearing after up to a few seconds ("blinking"), a phenomenon known from single-molecule recordings but also from few-molecule ensembles (*24*) (fig. S4).

To better understand the patterns of overall vesicle movements, we investigated the sum of all frames for each of the individual movies. Areas where vesicles moved randomly appeared blurred, whereas stationary vesicles induced "hot spots" (Fig. 3A, left panel). A number of movies also showed linear patterns, indicative of vesicle routes or "tracks" (Fig. 3A, right panel). Typically, the hot spots assembled in areas reminiscent of confocal images of the synaptic boutons (Fig. 3B); the tracks, however, seemed to form between such boutons. The pattern of summed staining was not due to random vesicle accumulations, because it was relatively stable throughout each movie (Fig. 3, B and C). We analyzed 8 to 10 movies clearly dominated by hot spots or tracks, respectively, and we observed, as expected, that the vesicles within spot-dominated areas (boutons) tended to be much less mobile (Fig. 3, D and E), exhibiting a behavior much closer to that in fixed neurons (fig. S3).

To investigate the nature of the hot spots, we performed a running average analysis of the movies. Unlike the vesicles, the hot spots appeared to be immobile and persistent (Fig. 4, A and B). We frequently observed vesicles moving into hot spots and remaining temporarily trapped (Fig. 4C). However, we also observed vesicles disappearing instantly from hot spots, a behavior that we attribute to either blinking or to moving out of the focal plane. The hot spots were occupied for about 22% of the time (Fig. 4D); 31% of the vesicles passed through a hot spot and individual vesicles remained for 16% of the time in hot spots on average (Fig. 4E). The large number and wide distribution of hot spots argues against their being release sites where the vesicles would dock, because in this preparation typically only one, and rarely two, small active zones (~200 nm diameter) are found per bouton (*25*). The hot spots are likely to be "pockets" in the synaptic vesicle clusters where the labeled vesicles are occasionally constrained, although the molecules involved in the synaptic vesicle cross-linking have yet to be clearly defined (*26*).

In general, synaptic vesicles are quite mobile, although their tendency to move nondirectedly generally impedes their effective translation. Our data support the recently proposed stick-and-diffuse model (*18*, *19*), in which the vesicles repeatedly bind and diffuse away from the cellular elements. Nevertheless, a strong flux of synaptic vesicles is present through the axons (Fig. 2F). To place vesicle movement in perspective, if only one vesicle passes through a bouton each second, in about 3 min the number of vesicles passed through equals the total number of vesicles in the bouton (*25*). This suggests that the boutons from the same axon may be strongly interlinked, with their (recently endocytosed) vesicles participating in a common "superpool."

We conclude that STED microscopy can be used to investigate fast biological processes in vivo. The relatively low count rates in our images were less problematic than one might have thought, because the small spot size (62 nm), similar to the size of the vesicles (40 nm), allowed vesicles to be treated as distinct bright objects, which were easily distinguished from the low background. We used low-pass filtering to increase the confidence of detecting photon clusters representing vesicles. However, with a better knowledge of the background statistics and more sophisticated mathematical methods such as maximum-likelihood estimation, it should be possible to identify vesicles without such filtering. Moreover, brighter samples, or more sensitive imaging, would allow for higher resolution, a larger field of view, and/or faster recordings. Besides using higher densities of fluorescent markers, two relatively obvious improvements would allow us to reach this goal: STED with continuous-wave beams (*27*) would increase the instant photon flux and detection with two opposing high-aperture lenses would double the detection efficiency (*28*). This would permit further improvement of the data, because faster recordings would facilitate automatic tracking at even higher densities, eventually allowing the rapid imaging of a multitude of intracellular processes in living cells.

### References and Notes


1. S. W. Hell, J. Wichmann, *Opt. Lett.* **19**, 780 (1994).
2. K. I. Willig, S. O. Rizzoli, V. Westphal, R. Jahn, S. W. Hell, *Nature* **440**, 935 (2006).
3. G. Donnert *et al.*, *Proc. Natl. Acad. Sci. U.S.A.* **103**, 11440 (2006).
4. E. Betzig *et al.*, *Science* **313**, 1642 (2006).
5. M. J. Rust, M. Bates, X. Zhuang, *Nat. Methods* **3**, 793 (2006).
6. S. T. Hess, T. P. K. Girirajan, M. D. Mason, *Biophys. J.* **91**, 4258 (2006).
7. S. W. Hell, *Science* **316**, 1153 (2007).
8. G. Donnert *et al.*, *Biophys. J.* **92**, L67 (2007).
9. M. Bates, B. Huang, G. P. Dempsey, X. Zhuang, *Science* **317**, 1749 (2007).
10. T. C. Sudhof, *Annu. Rev. Neurosci.* **27**, 509 (2004).
11. A. M. Aravanis, J. L. Pyle, R. W. Tsien, *Nature* **423**, 643 (2003).
12. S. P. Gandhi, C. F. Stevens, *Nature* **423**, 607 (2003).
13. E. A. Lemke, J. Klingauf, *J. Neurosci.* **25**, 11034 (2005).
14. A. W. Henkel, L. L. Simpson, R. M. A. P. Ridge, W. J. Betz, *J. Neurosci.* **16**, 3960 (1996).
15. K. Kraszewski, L. Daniell, O. Mundigl, P. De Camilli, *J. Neurosci.* **16**, 5905 (1996).
16. M. A. Gaffield, S. O. Rizzoli, W. J. Betz, *Neuron* **51**, 317 (2006).
17. R. Jordan, E. A. Lemke, J. Klingauf, *Biophys. J.* **89**, 2091 (2005).
18. M. Shtrahman, C. Yeung, D. W. Nauen, G. Q. Bi, X. L. Wu, *Biophys. J.* **89**, 3615 (2005).
19. C. Yeung, M. Shtrahman, X. L. Wu, *Biophys. J.* **92**, 2271 (2007).
20. Material and methods are available as supporting material on *Science* Online.
21. S. O. Rizzoli, R. Jahn, *Traffic* **8**, 1137 (2007).
22. V. Westphal, M. A. Lauterbach, A. Di Nicola, S. W. Hell, *N. J. Phys.* **9**, 435 (2007).
23. K. J. Darcy, K. Staras, L. M. Collinson, Y. Goda, *Nat. Neurosci.* **9**, 315 (2006).
24. P. Tinnefeld, V. Buschmann, K. D. Weston, M. Sauer, *J. Phys. Chem. A* **107**, 323 (2003).
25. T. Schikorski, C. F. Stevens, *J. Neurosci.* **17**, 5858 (1997).
26. S. O. Rizzoli, W. J. Betz, *Nat. Rev. Neurosci.* **6**, 57 (2005).
27. K. I. Willig, B. Harke, R. Medda, S. W. Hell, *Nat. Methods* **4**, 915 (2007).
28. S. Hell, E. H. K. Stelzer, *J. Opt. Soc. Am. A* **9**, 2159 (1992).


29. S.O.R is the recipient of a long-term fellowship from the Human Frontier Science Program. This work was supported in part by funds from the Gottfried Wilhelm Leibniz Program of the Deutsche Forschungsgemeinschaft to R.J., by a grant from the German Ministry of Research and Education (BMBF, Nanolive) to S.W.H., and by a grant from the German Ministry of Research and Education (BMBF, Nanolive, "Vesikelbewegungen durch Nanoauflösung") to S.O.R. We thank I. Herfort for assistance with cell culturing and A. Di Nicola for his custom data-acquisition-card. We also thank L. Kastrup, J. Keller, and A. Schönle for helpful discussions and for help with the software ImSpector. Finally, we thank B. Rankin for critical reading of the manuscript.


### Supporting Online Material

www.sciencemag.org/cgi/content/full/1154228/DC1
Materials and Methods
Figs. S1 to S4
References
Movie S1


17 December 2007; accepted 8 February 2008
Published online 21 February 2008;
10.1126/science.1154228
Include this information when citing this paper.